



**HAL**  
open science

# Space-Ground Coherent Optical Links: Ground Receiver Performance With Adaptive Optics and Digital Phase-Locked Loop

Laurie Paillier, Raphaël Le Bidan, Jean-Marc Conan, Géraldine Artaud,  
Nicolas Vedrenne, Yves Jaouën

## ► To cite this version:

Laurie Paillier, Raphaël Le Bidan, Jean-Marc Conan, Géraldine Artaud, Nicolas Vedrenne, et al.. Space-Ground Coherent Optical Links: Ground Receiver Performance With Adaptive Optics and Digital Phase-Locked Loop. *Journal of Lightwave Technology*, 2020, 38 (20), pp.5716-5727. 10.1109/JLT.2020.3003561 . hal-02899629

**HAL Id: hal-02899629**

**<https://hal.science/hal-02899629>**

Submitted on 15 Jul 2020

**HAL** is a multi-disciplinary open access archive for the deposit and dissemination of scientific research documents, whether they are published or not. The documents may come from teaching and research institutions in France or abroad, or from public or private research centers.

L'archive ouverte pluridisciplinaire **HAL**, est destinée au dépôt et à la diffusion de documents scientifiques de niveau recherche, publiés ou non, émanant des établissements d'enseignement et de recherche français ou étrangers, des laboratoires publics ou privés.

# Space-Ground Coherent Optical Links: Ground Receiver Performance With Adaptive Optics and Digital Phase-Locked Loop

Laurie Paillier, Raphaël Le Bidan, *Member, IEEE*, Jean-Marc Conan, Géraldine Artaud, Nicolas Védrenne and Yves Jaouën

**Abstract**—In the framework of high-data-rate free-space optical low Earth orbit satellite-to-ground communication, we investigate, by means of a refined end-to-end numerical model of the link, the performance of a coherent receiver that combines an adaptive optics system and a specific digital receiver architecture. The design of a fine carrier recovery stage based on a phase-locked loop is presented and its performance is characterized. The end-to-end model includes the impact of atmospheric turbulence, adaptive optics correction, laser phase noise and of the frequency mismatch between the transmit and receiver lasers. The results show that adaptive optics coupled with classical digital phase-locked loop techniques can provide a reliable solution to the problem of carrier frequency and phase tracking in coherent satellite-to-ground optical links, after prior coarse frequency estimation. The phase-locked loop converges after a few hundreds of microseconds and accurately tracks the phase fluctuations. The residual amplitude fluctuations and laser phase noise are shown to be the dominant impairments for the link performance.

**Index Terms**—Coherent receiver, digital phase-locked loop, adaptive optics, carrier synchronization, LEO, downlink.

## I. INTRODUCTION

**I**N terrestrial fiber-optic communication networks, coherent optical transmissions are nowadays a key solution to reach high data rates [1]. The coupling of phase modulation and coherent detection indeed facilitates wavelength division multiplexing (WDM) and, compared to direct detection, offers higher sensitivity as well as the possibility of using high-order modulation. Free-space inter-satellite communications links already benefit from the numerous advantages of using optical transmission rather than or in addition to radio-frequency communications, such as lower power consumption or higher bandwidth [2], particularly with coherent methods [3]. Furthermore, recent analytical [4] [5] and experimental [6] [7] studies have contributed to demonstrate the high potential of coherent receiver for high data rate satellite-to-ground communications. Several uplink, downlink or bilateral communications experiments between a ground station and low Earth orbit (LEO) and geostationary (GEO) satellites based on coherent receiver technology have already been established [8].

Both satellite-to-ground links and inter-satellite transmissions undergo strong Doppler effects due to the relative motion between the emitter and the receiver [9][10]. This results in a possibly large frequency shift of the incoming signal with respect to the local oscillator (LO) frequency which adds up to the natural frequency drift that exists between the transmit and receive lasers. Another major impediment for coherent detection is the random phase variations caused by laser phase noise. Accurate tracking of the carrier frequency and phase mismatch is thus required for correct demodulation. For inter-satellite links, optical phase-locked loops (OPLL) have been investigated as a natural solution for carrier synchronization [11][12]. However, in the context of space-to-ground links, the atmospheric channel introduces specific additional signal disturbances. All these impairments need to be accounted for in the receiver design for space-to-ground links.

Signal propagation through atmospheric turbulence randomly impairs, often significantly, the amplitude and phase of the optical wave [13]. As a result the mixing efficiency between the incoming signal and the LO oscillator collapses dramatically, which ultimately reduces the down-converted power. A state-of-the-art solution to mitigate the phase distortions induced by the turbulence consists in using an adaptive optics (AO) system to improve the spatial phase matching between the signals [8]. However the AO correction is not perfect and residual phase aberrations remain. Moreover, the random amplitude variations, called scintillation, also impair the received signal without being compensated for by the AO system. To design an effective carrier recovery strategy, a fine modeling of these turbulent effects is thus crucial. Previous works have studied the performance of ground-space coherent receivers based on statistical models of the turbulence [4][14]. Their conclusions clearly show the benefits of using coherent modulation schemes in this context. Yet open questions still remain concerning the feasibility of frequency and phase locking in the presence of realistic free-space optical (FSO) channel impairments.

A fully-analog solution combining an OPLL and an optical injection loop is presented in [9] to deal with Doppler frequency shifts up to 10 GHz for 10 Gb/s binary phase-shift keying (BPSK) transmission. However the study does not take into account the random amplitude fluctuations caused by the turbulence. Frequency and phase recovery in the digital domain by digital signal processing (DSP) techniques is another option. In [7] the authors describe a digital coherent

L. Paillier, J-M. Conan and N. Védrenne are with ONERA, DOTA, Paris Saclay University, F-92320 Châtillon, France e-mail: laurie.paillier@onera.fr  
 R. Le Bidan is with IMT Atlantique, Lab-STICC, UBL, 29238 Brest, France  
 G. Artaud is with CNES, 31400 Toulouse, France  
 Y. Jaouën is with LTCI, Télécom Paris, Institut Polytechnique de Paris, 91120 Palaiseau, France

receiver based on DSP techniques developed for fiber-optic networks, with application to a 10.45 km FSO horizontal link. Frequency offset compensation is done by performing a Fourier transform of the signal. Carrier phase synchronization relies on the  $M^{\text{th}}$ -power phase estimation algorithm. A similar approach to phase recovery is presented in [14]. Neither of these studies, however, specifically address the performance of the carrier synchronization algorithms.

For acquisition of signals with a possibly large initial frequency offset, as may arise in the present context, digital carrier synchronization usually proceeds in two steps [15]. First, a coarse frequency estimation stage reduces the initial frequency error to a small fraction of the symbol clock frequency, before any subsequent synchronization function can successfully begin. Ephemeride predictions may be used for this purpose, with possible assistance from a complementary feedforward frequency estimator, *e.g.* Fourier-transform based, or from a frequency-lock loop (FLL) [16]. A fine carrier recovery stage then follows, in charge of tracking the small residual frequency and phase mismatch with respect to the local oscillator during the pass of the satellite.

The objective of this paper is to provide precise performance evaluation of a coherent LEO-to-ground link, for a specific receiver architecture, by means of an end-to-end simulation model that includes fine modeling of propagation through turbulence, AO correction, laser phase noise and carrier frequency mismatch. A coherent FSO 10-Gb/s differentially-encoded BPSK system is considered. First, the design of the fine carrier recovery stage is presented. It is assumed that the initial frequency mismatch has been reduced to a residual frequency offset of no more than a few hundred of MHz by prior coarse frequency correction. Second, the performance of this architecture is evaluated using our end-to-end model.

The digital receiver architecture under consideration for fine frequency and phase tracking combines a digital phase-locked loop (DPLL) and a digital automatic gain control (AGC). The DPLL was selected as it is a reference carrier synchronization solution for RF satellite communications. One finds them in particular at the heart of the robust carrier tracking techniques used in global positioning satellite systems [17]. Feedforward synchronizers may be preferred if very high data rate and/or fast acquisition time are required. On the other hand DPLL have the ability to track any phase disturbance that may remain after coarse frequency correction, without the need for specific estimators, provided the corresponding phase error is not large.

The paper is organized as follows. The architecture and parameters of the LEO satellite downlink and AO under consideration are introduced in Part II, followed by a description of the atmospheric channel in the presence of AO correction. The digital receiver is presented in Part III, with a focus on the architecture and design of the selected DPLL-based fine carrier recovery sub-system. Communication performance in the presence of realistic propagation impairments is investigated in Part IV. Conclusion follows in Part V.

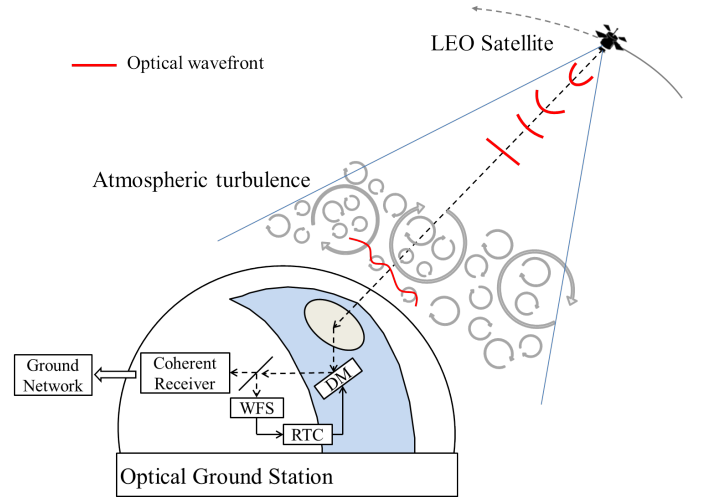


Fig. 1. General principle of a satellite-to-ground optical link with AO correction.

## II. MODELING OF A COHERENT LEO-TO-GROUND LINK

### A. Overall architecture

We consider a LEO-to-ground link having the overall architecture illustrated in Fig. 1 and Fig. 2. The transmitter at the LEO satellite is located several hundreds of km away from the optical ground station (OGS) receiver. Binary data are first differentially encoded, then transmitted with BPSK modulation of the phase of a continuous wave (CW) laser with the help of an electro-optic modulator (EOM) such as a Mach-Zehnder modulator. Compared to higher order modulation, the BPSK modulator is more convenient to integrate with the additional advantage of requiring less on-board power. The optical signal is then amplified by a booster amplifier and emitted in the direction of the OGS. The impact of the booster amplifier on the optical phase [18][19][20] will not be discussed in this paper. During free-space propagation through the atmosphere, the optical wave is severely degraded both in amplitude and in phase by the atmospheric turbulence.

On the ground, the incoming signal is mixed with the LO. An AO system is used to maximize the mixing efficiency and thus the down-converted coherent power by improving the spatial matching between the incoming and LO fields. In practice, the AO operates as follows [13]. A wavefront sensor (WFS) returns local information on the incoming wavefront. The WFS data are processed by the real-time computer (RTC) which controls the deformable mirror (DM) and adapts the surface of the latter so as to correct for the wavefront deformation. The resulting optical signal is then coherently detected by an intradyne receiver, sampled by an analog-to-digital converter (ADC), and demodulated by a baseband digital receiver whose architecture is described in Part III.

### B. Channel description and modeling

Variations of humidity and temperature in the atmosphere induce spatial and temporal random fluctuations of the refractive index of air. This phenomenon called atmospheric turbulence disturbs the amplitude and phase of the optical incident

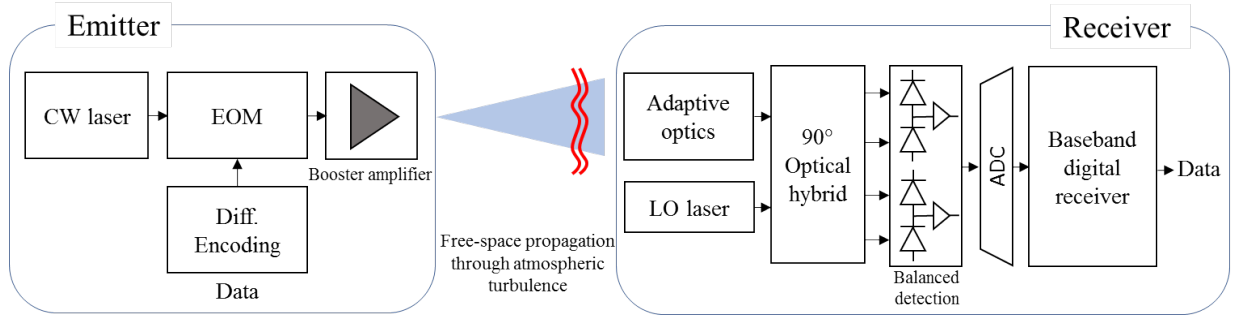


Fig. 2. Overall architecture of a LEO-to-ground communication link with coherent detection.

beam. The structure constant of refractive index fluctuations  $C_n^2(h)$  quantifies the local strength of the turbulence along the line of sight at different altitudes  $h$ , from the ground level to the maximum altitude  $h_{max}$  (here  $h_{max} = 20$  km). The  $C_n^2(h)$  profile used is derived from the Hufnagel-Valley profile [21] taken from the recommendation ITU-RP.1621-1. This model is parametrized by the value of the  $C_n^2$  at the ground level  $C_0$  and the high-altitude root-mean-square (RMS) wind speed parameter  $v_{RMS}$ . A Bufton wind profile [22] is considered here. The profile is defined by the wind speeds at the ground level  $v_G$  and at the tropopause  $v_T$ . The spatial coherence of the optical beam can be characterized by the Fried parameter  $r_0$ . This parameter gives information on the total turbulence strength along the line of sight. The scintillation index  $\sigma_I^2$  quantifies the point variations of power on the receiver pupil. Besides, the simulation also assumes a given outer scale  $L_0$  corresponding to the characteristic size of the larger eddies inducing the energy transfers in the atmosphere. The parameters characterizing the simulated turbulence are given in Table I. In the table, the Fried parameter and the scintillation index are given on the line-of-sight at the wavelength  $\lambda = 1550$  nm.

TABLE I  
LINK CHARACTERISTICS AND TURBULENT PARAMETERS FOR A  
LEO-TO-GROUND SCENARIO

Parameters	Values
Propagation wavelength $\lambda$	1550 nm
$C_0$	$10^{-13} \text{ m}^{-2/3}$
RMS wind speed parameter $v_{RMS}$	$20 \text{ m s}^{-1}$
Wind speed at the ground level $v_G$	$10 \text{ m s}^{-1}$
Wind speed at the tropopause $v_T$	$20 \text{ m s}^{-1}$
Fried parameter $r_0$	0.039 m
Outer scale $L_0$	5 m
Scintillation index $\sigma_I^2$	0.684
Elevation	20 deg
Satellite transverse velocity	$6.5 \text{ km s}^{-1}$
Rx aperture diameter $D_{RX}$	50 cm

The turbulent parameters are chosen to simulate a representative channel using data taken from the literature [23]. We consider that the communication with the LEO satellite is established at an elevation of 20 degrees to maximize the duration of the data transmission. Realistic temporal series of the propagated complex field are obtained using the end-to-

end propagation code TURANDOT developed by ONERA in cooperation with CNES [24]. In this method, the turbulent volume is sampled in discrete layers (here 35 layers) and a split-step algorithm performs Fresnel propagation between each discrete phase screen. The field entering the atmosphere at the altitude  $h_{max}$  is approximated by a plane wave considering the very large propagation distance from the satellite.

The complex field received within the telescope pupil plane is then sent to an end-to-end AO simulation. We assume that the correction modes are the Zernike polynomials (here up to mode 91, that is 12 radial orders) [25] [26]. The AO simulation models a closed loop at a given sampling frequency (here 5 kHz) with a 2 frame loop delay. The chosen AO design parameters are inspired from [27] and lead to an average flux penalty of -4.5 dB in the turbulent conditions described above. The WFS noise is neglected since requirements imposed by the data transmission lead to a high flux regime from the WFS point of view.

The electromagnetic field's complex amplitude of the incident beam after propagation through turbulence and correction with AO is characterized by :

$$E_{RX}(\mathbf{r}, t) = A_{TX} \exp(\chi(\mathbf{r}, t) + i\phi_{res}(\mathbf{r}, t)) \quad (1)$$

By definition of the complex amplitude [28], this equation does not include the term  $\exp(i\omega_{RX}t)$  with  $\omega_{RX}$  the wave pulsation. The factor  $A_{TX}$  is a function of the emitted power.  $\chi$  represents the log-amplitude fluctuation induced by scintillation and  $\mathbf{r}$  is the transverse two-dimensional spatial coordinate. The residual phase  $\phi_{res}$  corresponds to the residual phase perturbation due to the atmospheric turbulence  $\phi_{tur}$  after the AO phase correction  $\phi_{AO}$ :

$$\phi_{res}(\mathbf{r}, t) = \phi_{tur}(\mathbf{r}, t) - \phi_{AO}(\mathbf{r}, t) \quad (2)$$

The complex amplitude of the LO is represented by a Gaussian mode in the aperture plane [29] :

$$E_{LO}(\mathbf{r}) = A_{LO} \exp(-\|\mathbf{r}\|^2/w_0^2) \quad (3)$$

where  $A_{LO}$  is the constant amplitude of the LO and  $w_0$  is the mode radius. The mode radius is set to  $w_0 = \frac{D}{2.2}$  to maximize the efficiency while neglecting the central obscuration influence [30]. The LO power is denoted by  $P_{LO} = \frac{|A_{LO}|^2}{2}$ . Bi-dimensional scintillation and phase maps are illustrated in Fig. 3a and 3b. Turbulent phase residuals after AO correction is illustrated on Fig. 3c. Fig. 3d shows the Gaussian distribution

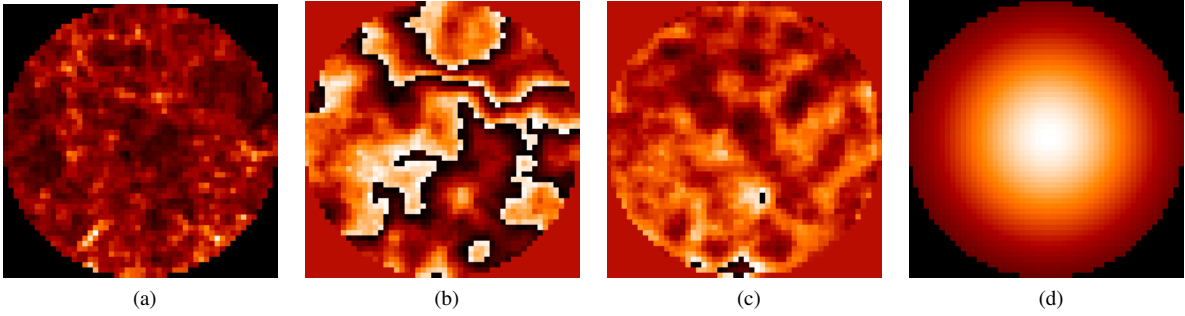


Fig. 3. a. Pupil amplitude map due to scintillation b. Turbulent phase in the pupil c. Residual phase after AO correction d. Amplitude of a Gaussian mode for  $w_0 = \frac{D}{2.2}$ . The phase maps are illustrated modulo  $2\pi$ .

of the LO mode projected in the aperture plane. The mixing efficiency between the incoming signal and the Gaussian mode of the LO is affected by the residual turbulence effect after the AO compensation. The instantaneous mixing efficiency can be derived from the complex coupling defined for instance in [31]. The complex coupling is an overlap integral expressed in the aperture plane, and reads:

$$C(t) = \int_P E_{LO}^*(\mathbf{r}, t) E_{RX}(\mathbf{r}, t) d\mathbf{r} \quad (4)$$

where the pupil transmittance  $P$  is defined by

$$P(\mathbf{r}) = \begin{cases} 1 & \text{if } 0 \leq 2\|\mathbf{r}\| \leq D_{RX} \\ 0 & \text{otherwise} \end{cases} \quad (5)$$

One can then define an instantaneous coupling efficiency  $\rho(t)$  [29] [32] and a phase noise  $\phi(t)$  in the form:

$$\rho(t) = |C(t)|^2 \quad (6)$$

$$\phi(t) = \arg(C(t)) \quad (7)$$

In the remainder of this section and for the ease of exposition, the modulated phase and the frequency mismatch are purposely omitted in the expression of complex amplitudes.

### C. Impact of the turbulence on the complex coupling

The simulation tool provides correlated time series of both the coupling efficiency and the turbulent induced phase noise in the considered turbulent conditions. The 2-seconds duration time series presented in this paragraph are those that will be used later in the end-to-end system simulation and performance evaluation described in part IV.

Fig. 4 presents the coupling efficiency  $\rho$  between the incident beam coming from the satellite and the local oscillator at the ground station, as defined by Eq. (6), with and without AO compensation, using the parameters described in Section II-B. As noted above, the frequency mismatch and the modulated phase are discarded, leaving only the turbulence induced fluctuations at the coherent detector output. Fig. 4 shows that the average flux penalty due to the turbulence is reduced from -23 dB to -4.5 dB thanks to the AO correction. Besides the cumulative density function and the probability density function (PDF) presented in Fig. 5 provide a quantification of the probability of fading occurrences and also prove that the system is effective at reducing the amplitude of the signal fluctuations.

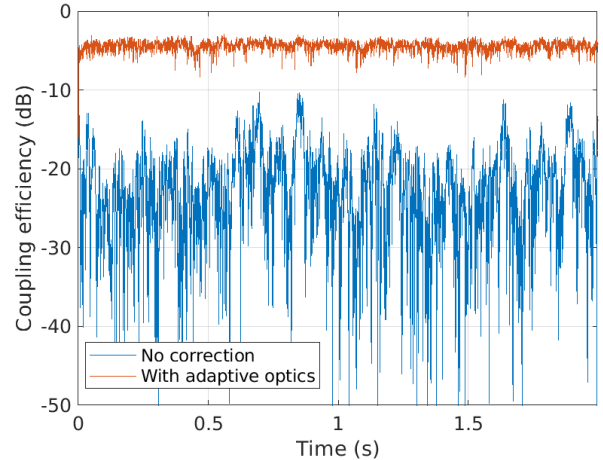


Fig. 4. Downlink 2 s duration time series of coupling efficiency. Comparison between a time series without correction and with an AO correction of 12 radial orders at the frequency of 5 kHz.

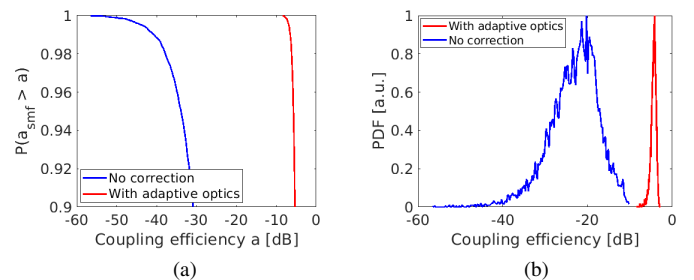


Fig. 5. Statistics of the coupled efficiency. a. Cumulative probabilities with and without AO correction b. Histogram of simulated coupling efficiency with and without AO correction (arbitrary unit).

Fig. 6a presents the turbulent phase noise corresponding to the atmospheric contribution to the phase noise  $\phi$  described in Eq. (7). BPSK modulation as well as other phase impairments due for instance to the Doppler effect or to the lasers instabilities are not represented here. Most of the residual phase noise after the AO correction can be attributed to the turbulent piston mode which is not corrected by traditional AO systems [33]. As shown on Fig. 6b the coherence time of the fluctuations is 70 ms in this case. This is slower than the phase noise fluctuations of the laser sources currently in use in terrestrial fiber networks. This is also much slower than the symbol rate

of 10 Gbaud. The practical impact of turbulence phase noise on the system performance will be evaluated in section IV-C.

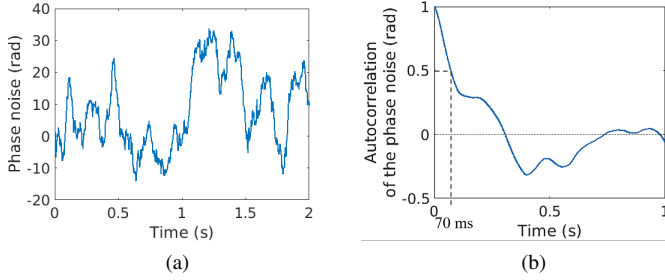


Fig. 6. a. Downlink 2 s duration time series of phase noise with an AO correction of 12 radial orders. b. Autocorrelation of the turbulent phase noise.

### III. COHERENT DETECTION AND DIGITAL BASEBAND RECEIVER PROCESSING

The coherent optical detection front-end and digital baseband receiver architecture are introduced in part III-A, followed by a detailed description of the proposed AGC and DPLL sub-systems in part III-B and III-C, respectively. A DPLL design example for FSO space-to-ground downlink communication is developed in part III-D, and validated with constant amplitude AWGN signal and laser phase noise in part III-E. Performance in the presence of turbulent amplitude fluctuations and turbulence-induced phase noise will be presented in part IV.

#### A. Coherent intradyne detection and digital receiver architecture

As shown in Fig. 2, after AO correction, the optical signal is sent to the coherent receiver and mixed with the LO signal for frequency down-conversion. Balanced detection produces an electrical signal which is sampled and digitized at twice or more the symbol rate  $1/T$ , where  $T$  denotes the symbol duration, and subsequently processed by the baseband digital receiver whose task is to recover the data bits as reliably as possible from the received samples sequence. The baseband digital receiver under consideration has the typical structure shown in Fig. 7. Here the coarse frequency correction stage is shown as part of the digital receiver but may also be analog or hybrid, in the form, for instance, of a feedback loop with the local oscillator.

During the pass of the satellite, the data signal experiences a frequency shift because of the Doppler effect and because of the natural frequency drift of the satellite laser source due to temperature variations for instance. The initial frequency error may be fairly large. The Doppler shift due to the relative speed of a LEO satellite with respect to the ground has been estimated in [9] to cover a total range of approximately 9 GHz (from -4.5 GHz to 4.5 GHz). It is the task of the coarse frequency correction to reduce the initial frequency mismatch between the transmit and receiver lasers down to a small fraction of the symbol clock frequency. At such an early stage in the receiver, channel state information is hardly available and

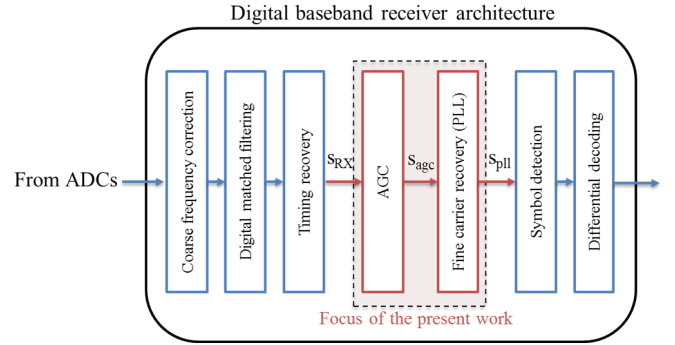


Fig. 7. Baseband digital receiver architecture under consideration.

symbol timing is unknown. An estimate of the Doppler shift can be obtained from the knowledge of the satellite trajectory, similarly to what is done in inter-satellites communications. The open-loop or closed-loop robust frequency acquisition schemes developed for RF communications may be used to further refine this estimate as well as to correct for the random frequency drift of the lasers, see *e.g.* [15, Sec. 5.3] or [16]. Alternatively, full optical PLL-based Doppler shift recovery could also be considered [9]. Coarse frequency correction will not be further discussed in this study, except for considerations of residual frequency error which is assumed to be well modeled by a constant frequency offset  $\Delta f = \frac{\Delta\omega}{2\pi}$  of the same order as those encountered in inter-satellite communication [11] [34]. Hereafter a maximum frequency offset of 100 MHz will be considered.

Once coarse frequency correction has ensured that most of the received signal falls within the bandwidth of the baseband receive filters, one can proceed to digital matched-filtering, timing recovery and symbol-rate down-sampling to obtain a sequence of  $T$ -spaced complex-valued samples  $s_{RX}(k) = s_{RX,I}(k) + i s_{RX,Q}(k)$  to be delivered to the decision circuit. Timing recovery will not be investigated in the following. Assuming perfect timing synchronization and ideal end-to-end Nyquist matched-filtering, the signal model for  $s_{RX}(k)$  is

$$s_{RX}(k) \propto \sqrt{\rho(k)} \exp(i(\Delta\omega kT + \varphi_m(k) + \theta(k))) + n(k) \quad (8)$$

where  $\varphi_m(k) \in \{0, \pi\}$  accounts for BPSK modulation and  $\theta(k)$  accounts for any residual phase mismatch, including:

- the turbulent phase noise after AO correction (see Fig. 6),
- the cumulative phase noise contribution from the transmit and receive laser sources,
- the static phase offset between the two lasers.

The cumulative laser phase noise is commonly modeled as a Wiener process and its spectrum approximated by a Lorentzian shape [35]. It mainly depends on the spectral linewidth  $\Delta\nu$  of the transmit and receive lasers, which corresponds to the full width at half maximum of its spectrum. Hereafter the spectral linewidth of each laser is considered to be 100 kHz [36] so that the total spectral linewidth of the phase noise is  $\Delta\nu = 200$  kHz. The time-varying amplitude factor  $\sqrt{\rho(k)}$  can be related to the usual  $\sqrt{P_{RX}P_{LO}}$  term that appears in the coherent detection equations, with  $P_{RX}$  the received power from the satellite. One can note that the term  $\rho(k)$  corresponds

to the coupling efficiency defined by Eq. (6) and illustrated in Fig. 4. In the following, the coupling efficiency  $\rho$  as well as the turbulence phase noise are supposed to be approximately constant within a symbol period  $T$ , which, according to Fig. 4 and Fig. 6, is a reasonable assumption for a 10-GBaud link. Finally,  $n(k) = n_I(k) + i n_Q(k)$  is the discrete-time complex additive noise. The LO power is assumed to be larger than the receive signal power so that shot noise dominates. Denoting by  $N_0$  the one-sided power spectral density of shot noise [37] and assuming that time shifts of the receive filter by integer multiples of the symbol period  $T$  form an orthonormal basis,  $n_I(k)$  and  $n_Q(k)$  are well-modeled as two independent, zero-mean white Gaussian random variables with variance  $N_0/2$ .

The role of the subsequent fine carrier recovery stage is to track and compensate for the residual frequency offset  $\Delta\omega$  and phase mismatch  $\theta(k)$  in Eq. (8), in order for the BPSK decision circuit to recover the data bits with minimum probability of error. Motivated by common practice in the field of RF space-to-ground satellite communication, we propose to use a DPLL for that purpose since a properly-designed DPLL has the inherent ability to track any residual phase or frequency error provided it is not too large. In the proposed receiver architecture, the DPLL is preceded by an AGC whose role is to maintain the received signal power at a constant target value. In the next sub-sections the emphasis will be placed on the design of the AGC and DPLL subsystems since both play a key role in addressing the various impairments that affect the received coherent signal.

A BPSK symbol detector and a differential decoder follow, to recover the transmitted bits from the discrete-time samples at the DPLL output. These two operations are standard practice in communication systems and will not be further discussed.

### B. Digital automatic gain control architecture

The role of the digital AGC is to maintain a constant average received signal power. A closed-loop digital AGC has been used in the present work, with the structure shown in Fig. 8.

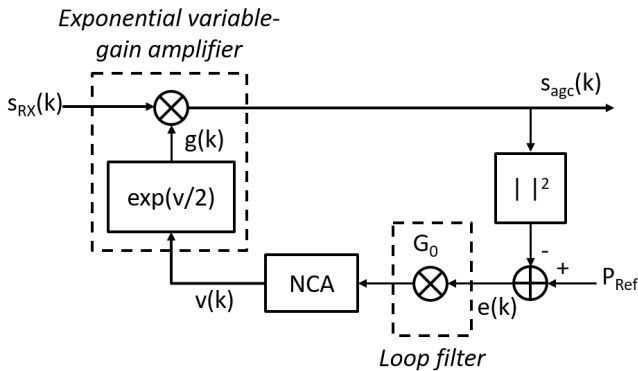


Fig. 8. Block diagram of the digital automatic gain control loop.

First, the instantaneous signal power is computed and compared to the target reference power  $P_{\text{Ref}}$  to form the driving error signal

$$e(k) = P_{\text{Ref}} - |s_{\text{agc}}(k)|^2 \quad (9)$$

A unit average power  $P_{\text{Ref}} = 1$  was chosen as reference. The error signal  $e(k)$  is weighted by a constant factor  $G_0 > 0$  which plays the role of the loop filter here, and then passed through a linear numerically controlled amplifier (NCA) implemented as a unit-gain first-order integrator with transfer function  $1/(z - 1)$ . The linear NCA is followed by an exponential transform to create a variable-gain amplifier with exponential gain control characteristic  $g(k) = \exp(v(k)/2)$ , where  $v(k)$  is the linear gain control voltage at the output of the NCA. The exponential characteristic ensures that the acquisition time only depends on the loop parameters, and not on the dynamics of the input signal [38]. The gain factor  $g(k)$  is finally applied to the received sample  $s_{\text{RX}}(k)$  to regulate the signal level fluctuations. In our experiments, the AGC gain was set to  $G_0 = 0.1$  as a trade-off between stability and convergence speed of the loop.

In the absence of additive noise, the complex signal at the output of the AGC loop can be written as:

$$s_{\text{agc}}(k) = A_{\text{agc}}(k) \exp(i(\varphi_m(k) + \varphi(k))) \quad (10)$$

with  $\varphi(k) = \Delta\omega kT + \theta(k)$  the total phase offset to be recovered by the fine carrier recovery stage.

### C. Digital phase-locked loop architecture

The purpose of the DPLL is to generate a discrete-time replica signal whose phase and frequency are synchronized with the incoming signal. The DPLL does this by driving to zero the tracking error  $\Delta\varphi = \varphi - \hat{\varphi}$  between the phase  $\varphi$  of the incoming signal from the AGC and the phase estimate  $\hat{\varphi}$  computed by the DPLL. Fig. 9 shows the block diagram of the DPLL. The loop consists of 3 sub-blocks: a phase detector, a loop filter, and a numerically-controlled oscillator (NCO).

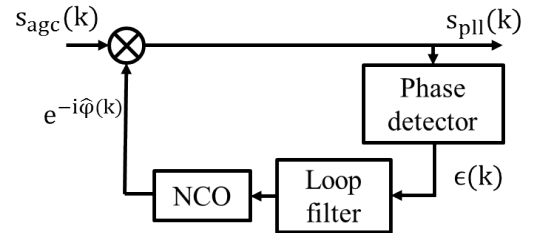


Fig. 9. Block diagram of the digital phase locked loop.

The phase detector (PD) sub-block in Fig. 9 aims at estimating the tracking error  $\Delta\varphi(k) = \varphi(k) - \hat{\varphi}(k)$  for the  $k$ th sample. The optimal non-data-aided maximum a posteriori (MAP) PD for closed-loop estimation of an unknown carrier phase offset affecting a BPSK modulated signal is [39]:

$$\epsilon(k) = s_{\text{pll},Q}(k) \tanh(s_{\text{pll},I}(k)) \quad (11)$$

with

$$s_{\text{pll},I}(k) = A_{\text{agc}} \cos(\varphi_m(k) + \Delta\varphi(k)) \quad (12)$$

$$s_{\text{pll},Q}(k) = A_{\text{agc}} \sin(\varphi_m(k) + \Delta\varphi(k)) \quad (13)$$

in the absence of noise. Ideal AGC is assumed in the above signal model, so that  $A_{\text{agc}}(k) = \sqrt{P_{\text{Ref}}} = A_{\text{agc}} \forall k$ . The impact

of non-ideal AGC on the DPLL design is discussed later in part III-D. In the remainder of this paper, we have chosen to work with the low signal-to-noise ratio (SNR) approximation of the optimal MAP PD obtained from  $\tanh(x) \approx x$  and which reads [40]:

$$\epsilon(k) = s_{\text{pll},I}(k) s_{\text{pll},Q}(k) \quad (14)$$

The latter is commonly referred to as *Costas-type* or  $I \times Q$  PD as it mimics the operation of an analog Costas loop. This choice for the PD was motivated by the desire to capitalize on the significant amount of literature and results available for performance analysis of Costas-type PLLs in both the linear and non-linear regimes, as well as to ensure robust operation of the DPLL in the presence of fadings. From Eq. (12), (13) and (14), one obtains that the Costas-type PD has a sinusoidal S-curve characteristic with period  $\pi$ , since:

$$\epsilon(k) = \frac{A_{\text{agc}}^2}{2} \sin(2(\varphi_m(k) + \Delta\varphi(k))) \quad (15)$$

$$= \frac{K_d}{2} \sin(2\Delta\varphi(k)) \quad (16)$$

where  $K_d = A_{\text{agc}}^2$  is the phase detector gain. From (16), a linear approximation of the Costas-type PD output valid for small tracking error  $\Delta\varphi(k)$  is

$$\epsilon(k) \approx K_d \Delta\varphi(k) \quad (17)$$

The output of the PD is smoothed by a second-order loop filter having gains  $K_1$  and  $K_2$  and discrete-time transfer function:

$$F(z) = K_1 \left( 1 + \frac{K_2}{z-1} \right) \quad (18)$$

The loop filter output is used to drive the NCO which generates in turn a replica whose phase is close to that of the incoming signal. Here the NCO is implemented as a unit-gain, first-order integrator with transfer function  $1/(z-1)$  followed by a discrete-time complex phase rotator.

Designing the DPLL requires choosing the gain coefficients  $K_d$ ,  $K_1$  and  $K_2$ . Since for the Costas-type PD we have  $K_d = A_{\text{agc}}^2$ , knowledge of the average incoming signal power is thus required in the DPLL design. A unit average power will be assumed in the remainder of this paper, an hypothesis reinforced by the digital AGC frond-end, resulting in  $K_d = 1$ . Then only  $K_1$  and  $K_2$  need to be specified. To this end, it is common practice to assume that the DPLL operates in steady-state tracking mode, with a tracking error  $\Delta\varphi$  small enough that the DPLL can be described as a linear system whose transfer function can be calculated. One can then resort to three intermediate variables that have more physical relevance, namely: the damping factor  $\xi$ , the loop noise-equivalent bandwidth  $B_L$ , and the natural frequency  $\omega_n$ . Those parameters were originally introduced for analog PLLs [41]. By transposing this approach to the digital domain and from the linear approximation (17) of the Costas-type PD, we obtain the following discrete-time equivalent formulas for our three parameters of interest

$$B_L T = \frac{1}{4}(K + K_2) = \frac{K}{4} \left( 1 + \frac{1}{4\xi^2} \right) \quad (19)$$

$$\xi = \frac{1}{2} \sqrt{\frac{K}{K_2}} \quad (20)$$

$$\omega_n T = \sqrt{K K_2} = \frac{K}{2\xi} \quad (21)$$

where  $K = K_d K_1 K_0$  denotes the global loop gain. As noted in [41] the analog formulas are good approximations for the DPLL parameters as long as  $\omega_n$  is small compared to the sampling rate  $1/T$ . It is common practice to assign the value  $\xi = \frac{1}{\sqrt{2}}$  to the damping factor as a good trade-off between stability of the loop and speed of convergence [41]. DPLL design then reduces to selecting an appropriate value for the normalized loop bandwidth  $B_L T$ , or equivalently for the normalized natural frequency  $\omega_n T$  (the two parameters play an equivalent role in the design, albeit with different physical interpretation), to obtain the corresponding loop gain  $K_1$  and  $K_2$ . We shall now briefly sketch one possible way to proceed for the present communication scenario.

#### D. DPLL design example

Having set  $\xi = \frac{1}{\sqrt{2}}$ , we are left with two degrees-of-freedom in the DPLL design: choice of the loop equivalent bandwidth  $B_L$ , and choice of the sampling rate  $1/T$ . The later is often primarily governed by hardware considerations. In the following, we make the usual assumption that the DPLL sampling rate is equal to the symbol rate, 10 Gbaud in the present case. Given the sampling rate, the choice of the loop equivalent bandwidth  $B_L$  is driven by several considerations:

- 1) ensuring that the DPLL can lock onto the maximum residual frequency offset expected after coarse frequency correction, with an acquisition time much smaller than the ground station acquisition time, which is in the order of a few seconds ;
- 2) limiting the BER penalty due to residual tracking errors at the DPLL output ;
- 3) preventing as much as possible cycle slipping and loss of lock during the satellite pass

The design procedure to be described below prioritizes design objective 2), and also objective 3) but to a lesser extent. In the presence of additive white gaussian noise, the tracking error or phase jitter  $\Delta\varphi$  at the DPLL output is a random process whose variance  $\sigma_{\Delta\varphi}^2$  at high enough SNR is given by [39]

$$\sigma_{\Delta\varphi}^2 = \frac{B_L T}{E_s/N_0} \times \left( 1 + \frac{1}{2E_s/N_0} \right) \quad (22)$$

This expression assumes a locked DPLL operating in steady-state condition so that the linear approximation (17) of the PD output holds.  $E_s/N_0$  is the electrical SNR, with  $E_s$  the average received energy per symbol and  $N_0$  the one-sided noise power spectral density. One recognizes in the first term of (22) the Cramer-Rao bound (CRB) for closed-loop estimation of an unknown phase offset affecting a constant amplitude sinusoidal signal without phase modulation:

$$\sigma_{\text{CRB}}^2 = \frac{B_L T}{E_s/N_0} \quad (23)$$

BPSK modulation induces a penalty on the previous bound, the so-called squaring-loss penalty, which for the Costas-type

PD is reflected into the second factor in (22) [39]. Laser phase noise also has an impact on the phase jitter, translating into an additional term in  $\sigma_{\Delta\varphi}^2$  which becomes [42]:

$$\sigma_{\Delta\varphi}^2 = \frac{B_L T}{E_s/N_0} \times \left(1 + \frac{1}{2E_s/N_0}\right) + \pi\Delta\nu T \left(\frac{1 + \frac{1}{4\xi^2}}{4B_L T}\right) \quad (24)$$

Following the conclusions obtained in Part II, we assume that the turbulence-induced phase noise has negligible contribution in the total phase jitter compared to the other noise sources. From (24) one observes that setting  $B_L$  is the result of a trade-off between improving the tracking capability of the laser phase noise fluctuations and reducing the DPLL sensitivity to additive noise. Phase jitter increases the probability of loss of lock and simultaneously degrades the BER performance by introducing a random phase offset at the decision point. By designing the DPLL so that the total phase jitter does not exceed a certain maximum angle, one may limit these detrimental effects.

Given a statistical model for the distribution  $f(\Delta\varphi)$  of the phase jitter, one possible way to proceed is to first evaluate the average theoretical BER in the presence of random tracking errors at the DPLL output as

$$\bar{P}_b = \mathbb{E}_{\Delta\varphi} [P_b(\Delta\varphi)|\Delta\varphi] = \int_0^{2\pi} P_b(\Delta\varphi) f(\Delta\varphi) d(\Delta\varphi) \quad (25)$$

with  $P_b(\Delta\varphi)$  the analytical BER in the presence of a static phase offset  $\Delta\varphi$ . Note that  $\bar{P}_b$  is a function of the SNR  $E_s/N_0$  and jitter noise variance  $\sigma_{\Delta\varphi,\max}^2$ . Different jitter variances will result in different average BER at a given SNR, or, equivalently, in different SNR values (or different SNR penalties with respect to the performance without phase jitter) at a given BER. One may then 1) decide a target BER and maximum tolerable SNR penalty at this BER from design or system requirements, 2) use Eq. (25) to convert this maximum tolerable SNR penalty at the target BER into a maximum tolerable jitter variance  $\sigma_{\Delta\varphi,\max}^2$  at the DPLL output, and 3) set  $B_L$  accordingly from (24). For the present design example, the target BER after demodulation was set to  $10^{-4}$  to ensure Quasi-Error-Free performance after forward-error correction [43, Table I]. For differentially-encoded BPSK in AWGN, this corresponds to an operating SNR  $E_s/N_0 \approx 8$  dB (see "AWGN channel" curve in Fig. 15). A maximum tolerable SNR penalty due to phase jitter of 0.1 dB was selected, to illustrate the principle, and a Tikhonov distribution was assumed for the phase jitter statistics [44]. Then Eq. (25) gives us a maximum tolerable jitter variance  $\sigma_{\Delta\varphi,\max}^2 = 0.02$  rad<sup>2</sup>, or equivalently a maximum standard deviation  $\sigma_{\Delta\varphi,\max} = 8^\circ$ . Considering a cumulated 3-dB laser linewidth  $\Delta\nu = 200$  kHz, we find from (24) that a noise-equivalent bandwidth  $B_L = 12$  MHz is needed, yielding the DPLL configuration in Table II.

Once a value for  $B_L$  has been obtained, we have to make sure that it meets all other requirements, in particular design objective 1). We first note that  $B_L = 12$  MHz corresponds to a natural frequency  $\omega_n = 22.6 \times 10^6$  rad/s. The condition  $\omega_n \ll 1/T$  required for designing the DPLL based on formulas initially derived for analog PLLs is thus fulfilled. A second-order analog PLL with Costas-type PD and perfect integrator

TABLE II  
PHASE-LOCKED LOOP MAIN PARAMETERS

Parameters	Values
$T$	0.1 ns
Damping factor	$\frac{1}{\sqrt{2}}$
Loop bandwidth $B_L$	12 MHz
$K_1$	$3.2 \cdot 10^{-3}$
$K_2$	$1.6 \cdot 10^{-3}$
Sampling rate	10 GHz

in the loop filter is known to have infinite hold-in range and pull-in range (in the absence of Doppler rate), which means that the loop is theoretically able to compensate for any initial frequency offset provided it is given enough time to do so. Caution is required, though, when transposing these notions to the digital domain. Considering a Costas-type PD, a DPLL will no longer be able to accurately track the error and eventually lose lock if the phase jump between two successive samples exceeds  $\pi/2$ . This translates into a maximum frequency offset of 2.5 GHz in the present configuration, which is far beyond the expected residual frequency mismatch. More meaningful is the pull-in time, which is a good measure of the time required by the loop to establish the lock. Adopting the same approach as before and transposing the pull-in time definition for analog loops into the digital domain [41], we obtain the following acquisition time prediction for an initial frequency offset  $\frac{\Delta\omega}{2\pi}$ :

$$T_p = \frac{2\Delta\omega^2}{\xi\omega_n^3} \quad (26)$$

which, in the present case, gives  $T_p \approx 96$   $\mu$ s for a frequency offset of 100 MHz. This is much shorter than the ground station acquisition time, in the order of a few seconds. In addition to conditioning the acquisition range and convergence speed of the loop, the normalized loop bandwidth  $B_L T$  also determines to a large extent the sensitivity of the loop to cycle slips caused by noise. For the present design,  $B_L T = 0.0012$  which is small enough to reasonably assume that the probability of cycle slips occurrence during the satellite pass is close to zero. Mathematical analysis of cycle-slipping is notoriously difficult. An estimate of the average mean time  $T_c$  between slips for a DPLL with a period- $p$  sinusoidal S-curve, valid at low SNR, is provided in [45] as

$$T_c = \frac{\pi}{4B_L} \exp\left(\frac{p^2}{\pi^2 \sigma_{\Delta\varphi}^2}\right) \quad (27)$$

which gives  $T_c \approx 3.4 \times 10^{14}$  s for the present design, suggesting comfortable margin.

Several final comments are in order here. First, assuming a DPLL running at a sampling rate of 10 GHz might appear somewhat optimistic in view of current hardware capabilities. Practical implementation may operate at 1 GHz or even slower, by adapting the DPLL design accordingly, albeit with inferior acquisition and tracking capabilities. In particular the loop bandwidth  $B_L$  will have to be increased accordingly and the corresponding impact on the system performance needs to be assessed. Second, the DPLL design method described

previously assumes a unitary PD gain  $K_d = 1$ , and thus a constant (short-term) average received power as a consequence of the choice of a Costas-type PD. A digital AGC precedes the DPLL to reinforce this assumption. However, in practice the AGC is not perfect and additive noise remains so that the received power still fluctuates. In the case of strong residual fluctuations, the DPLL performance is hard to predict without resorting to end-to-end simulations similar to the one used in part IV. We note from (19) that fading will reduce the loop bandwidth  $B_L$ , which enhances AWGN robustness but also increases phase noise sensitivity at the same time. Fading will also increase the convergence time  $T_p$ . One of the main reasons for selecting a Costas-type PD was its proven optimality (at low SNR). The latter however assumes constant-amplitude BPSK signals in AWGN. More robust PD may thus exist, with better performance in the presence of random, time-varying amplitude variations. A possible alternative could be the arctan PD  $\epsilon(k) = \arctan(s_{\text{pll},Q}(k)/s_{\text{pll},I}(k))$  which is independent of the signal level. Other approaches such as variable-bandwidth PLLs based on Kalman filters are discussed in [17]. We leave here this question open for further work.

#### E. PLL characterization without turbulence

Fig. 10 shows the acquisition phase of the presented system in the presence of AWGN only, at an SNR of 8 dB. Here, the loop locks onto an initial frequency offset  $\Delta f = 100$  MHz after 104  $\mu\text{s}$ . The DPLL is thus able to acquire the target frequency shift in a reasonable time compared to the ground station acquisition time. Furthermore and as expected, the measured acquisition time is in accordance with the prediction  $T_p \approx 96 \mu\text{s}$  obtained from Eq. (27).

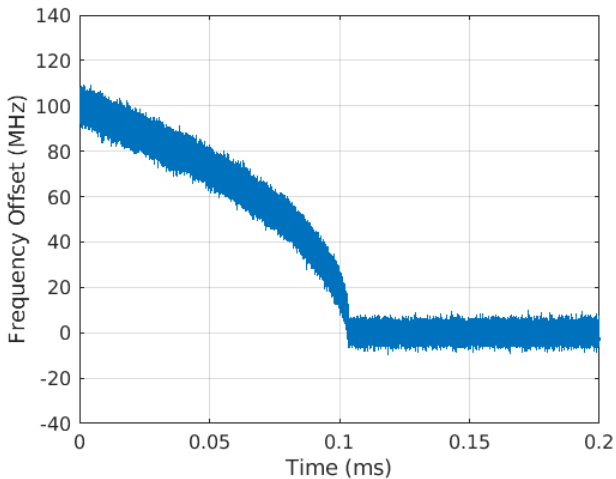


Fig. 10. Frequency offset evolution during lock-in at SNR  $E_s/N_0 = 8$  dB.

To validate further the behavior of the DPLL, we have plotted in Fig. 11 the tracking error variance  $\sigma_{\Delta\varphi}^2$  as a function of SNR in steady-state performance (transients occurring during the acquisition period have been excluded from the calculation) with and without laser phase noise. In both cases, we first note the existence of a minimum SNR value, here around -7 dB for AWGN only, and -5 dB for AWGN and

laser phase noise, under which the DPLL is unable to lock and becomes unstable. Above this critical SNR value, the measured tracking error variance quickly converges towards the theoretical bound given by Eq. (22) and (24). This validates our design. At SNR values lower than the critical SNR, the previous design assumptions and formulas no longer apply since the DPLL operates in a highly non-linear regime and proves to be unable to reach a stable state. However we do not expect the system to operate in such conditions.

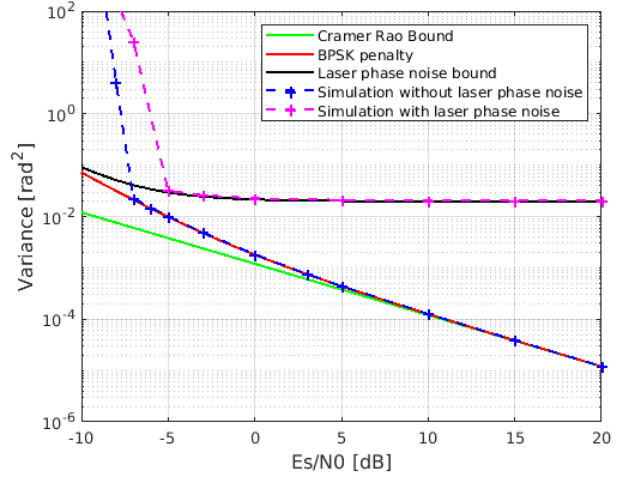


Fig. 11. Variance of the tracking error at the DPLL output as a function of SNR, with and without laser phase noise ( $\Delta\nu = 200$  kHz), and comparison with the theoretical bounds (initial frequency offset  $\Delta f = 100$  MHz).

## IV. SYSTEM PERFORMANCE WITH ADAPTIVE OPTICS

Having validated the proposed fine carrier recovery subsystem in the ideal case of a BPSK modulated signal impaired by AWGN and laser phase noise only, we now investigate its robustness in more realistic propagation conditions based on the FSO link model described in Section II, more precisely on the simulated time series obtained after AO correction and presented in Fig. 4 and 6, respectively. First the role of the AGC loop in such an uncertain environment is highlighted. Then we characterize the convergence and tracking performance of the DPLL in the presence of residual amplitude fluctuations, turbulent phase noise and laser phase noise. We finally evaluate the BER performance of the overall transmission system.

### A. Fluctuations mitigation with automatic gain control

The main purpose of the digital AGC is to compensate for the slow residual amplitude fluctuations caused by atmospheric turbulence that remain after AO correction. A unit target reference power  $P_{Ref} = 1$  is used in the loop so as to match the assumption of unit phase detector  $K_d = 1$  used in the DPLL design (see Section III-C.D), thereby ensuring that the loop will run in nominal operating conditions. Fig. 12 shows the impact of the AGC on the received signal power variations. Note that the multiplicative gain of the AGC loop impacts equally the signal and the noise. In particular, during fades, both the signal and the noise are amplified.

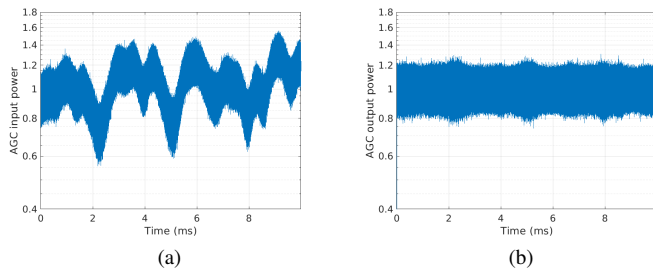


Fig. 12. 10 ms duration time series of the AGC (a) input and (b) output power at an average SNR of 30 dB (value chosen for illustration purpose only).

### B. Digital frequency shift compensation

After the AGC loop the signal is sent to the PLL. Fig. 13 presents the acquisition step of the PLL at an average SNR of 8 dB. The initial frequency offset between the incoming signal and the LO was set to 100 MHz again. It is interesting to note that despite the residual amplitude fluctuations, the theoretical prediction still applies since the DPLL requires again  $T_p \approx 106 \mu\text{s}$  only to converge. This confirms that with proper prior AO correction and AGC compensation, the proposed digital PLL can maintain very short lock-in time compared to the ground station acquisition time even in turbulent conditions.

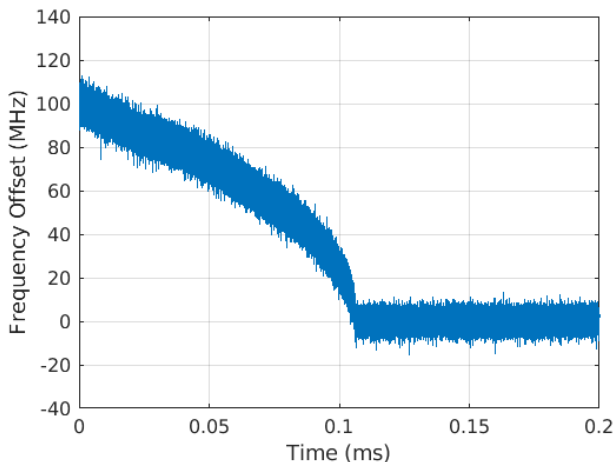


Fig. 13. Frequency error during the lock-in process. Temporal series with a mean SNR of 8 dB.

Fig. 14 shows the evolution of the variance of the tracking error at the DPLL output (excluding the acquisition period) with and without laser phase noise, as a function of the average SNR on the overall time series. The results are compared to the theoretical expressions given in Eq. (22) and in Eq.(24) which were derived for a constant amplitude signal and analog loop. The main impact of fading is to increase the minimal critical SNR value under which the DPLL becomes unstable. By comparing Fig. 11 and Fig. 14, the penalty is approximately 5 dB with turbulence only, and is more important, around 10 dB, in the presence of laser phase noise. In all cases, however, the results closely match the corresponding bounds at average SNRs of 8 dB and higher. This proves that the

DPLL is able to maintain the lock and accurately track the residual phase fluctuations even in the presence of turbulence.

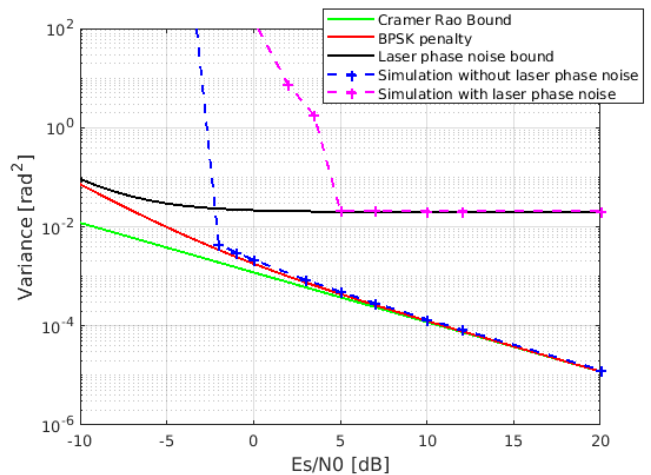


Fig. 14. Tracking error variance at the DPLL output as a function of average SNR for an initial frequency offset  $\Delta f = 100$  MHz and the 2 s-duration time series, with and without laser phase noise ( $\Delta\nu = 200$  kHz).

### C. Impact of turbulent phase noise after adaptive optics correction

The simulation presented in Fig. 14 has been done in the presence of the residual amplitude fluctuations and turbulent phase noise after AO correction. We observe that the tracking error variance measured at the DPLL output is superimposed on the theoretical bound at high SNR which proves that the turbulent phase noise has no impact on the results.

### D. BER performance

After the DPLL, BPSK symbol detection is performed, followed by differential decoding in order to remove the phase ambiguity which may subsist when the PLL locks onto an incorrect phase due to the rotational symmetry of the PSK constellation. Fig. 15 shows the simulated BER performance of the space-to-ground downlink for the 2 s-duration time series presented in Fig. 4 and Fig. 6a. The frequency offset was set to 100 MHz. The BER is calculated once convergence is obtained. The results are compared with and without laser phase noise, to assess the impact of the latter. For reference purpose we have also included the performance over AWGN without frequency offset, with and without laser phase noise again. Also shown is the performance obtained in the presence of turbulence only, without frequency offset nor laser phase noise. We first note that the BER performance is virtually the same with and without frequency offset. This demonstrates the capability of the selected digital fine carrier recovery solution to correct for the target frequency offset without BER penalty. By comparing the performance with and without turbulence, all other things being equal, the residual fading caused by atmospheric turbulence result in a 2.3 dB power penalty at a  $\text{BER}=10^{-4}$ . Finally, an SNR gap of about 0.1 dB is observed between the performance with and without laser phase noise at  $10^{-4}$ , either in AWGN only or in the presence of turbulence, thereby validating the design method suggested in Part III.D.

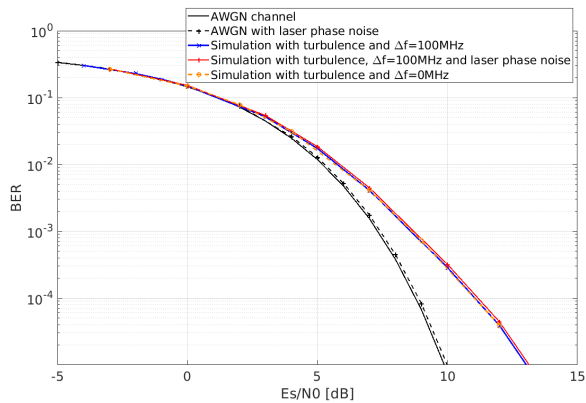


Fig. 15. BER performance as a function of the average SNR.

## V. CONCLUSION

Coherent receivers are gradually emerging as a key enabler for high-data-rate communications not only in fiber-optics networks but also in free-space optical communications. In this paper, we have investigated end-to-end link modeling and digital receiver design for a particular example of receiver architecture, for coherent 10 Gb/s BPSK LEO satellite-to-ground FSO transmission in the presence of realistic atmospheric turbulence, AO correction, laser phase noise and frequency mismatch. At the ground station, AO correction is used to improve the mixing efficiency of the incoming signal with the LO and to achieve an average flux penalty of -4.5 dB. The impact of the propagation and AO correction on the phase noise has also been characterized. The design of a fine carrier recovery stage which combines an AGC with a DPLL is described in order to recover from the frequency offset and track residual phase variations after intradyne detection. The overall system performance has been characterized based on realistic time series of a representative LEO-to-ground link with AO correction obtained from end-to-end simulations in the presence of laser phase noise and frequency offset.

The digital receiver is able to acquire and track a frequency offset of 100 MHz in approximately 100  $\mu$ s, a reasonable amount of time compared to the few seconds required for establishing the satellite link. This compensation is done without BER penalty with respect to the ideal case of a perfectly synchronized LO. We however show that amplitude fluctuations degrade the BER performance. We also demonstrate that the turbulent phase noise has negligible impact on the carrier synchronization process. The laser phase noise is the predominant source of phase error. Its impact on the BER performance can be contained through careful PLL design or by the use of higher-quality lasers. For the specific receiver taken here as an example, the total power penalty induced by turbulence and laser phase noise at a BER= $10^{-4}$  is approximately 2.4 dB.

This paper therefore shows that AO coupled with a classical, DPLL-based carrier recovery stage can be a simple, robust solution to the problem of carrier frequency and phase tracking in coherent satellite-to-ground FSO links.

Here a DPLL was chosen as an example but the previous

conclusion is expected to extend to other standard algorithms as well, e.g. feedforward estimators. In particular, the performance and robustness of the open-loop carrier synchronization algorithms currently in use in fiber-optics networks could be investigated. In addition, one could investigate the requirements on the fading amplitude, and thus on the AO system design, so that the digital receiver operates properly. Different requirements may arise, depending on the selected DSP algorithms. Also, the DPLL was specifically designed for BPSK modulation in this work. The same methodology can however be extended to higher-modulation formats by modifying accordingly the phase detector function within the loop. Finally, this work assumed ideal timing recovery. In practice the latter will also be impaired by the Doppler effect and by the signal fadings prompting the need for robust digital symbol synchronization algorithms.

## ACKNOWLEDGMENT

This work was conducted in the framework of a PhD thesis co-funded by ONERA and CNES.

## REFERENCES

- [1] P. J. Winzer, D. T. Neilson, and A. R. Chraplyvy, "Fiber-optic transmission and networking: the previous 20 and the next 20 years," *Opt. Express*, vol. 26, no. 18, pp. 24 190–24 239, 2018.
- [2] H. Kaushal and G. Kaddoum, "Optical communication in space: challenges and mitigation techniques," *IEEE Commun. Surveys Tuts.*, vol. 19, no. 1, pp. 57–96, 2016.
- [3] F. Heine, G. Mühlwinkel, H. Zech, S. Philipp-May, and R. Meyer, "The european data relay system, high speed laser based data links," in *7th IEEE Adv. Satellite Multimedia Sys. Conf. and 13th Signal Proc. for Space Commun. Workshop (ASMS/SPSC)*, 2014, pp. 284–286.
- [4] A. Belmonte and J. M. Kahn, "Capacity of coherent free-space optical links using atmospheric compensation techniques," *Opt. Express*, vol. 17, no. 4, pp. 2763–2773, 2009.
- [5] —, "Satellite downlink coherent laser communications," in *Optical Wireless Communications*. Springer, 2016, pp. 325–343.
- [6] R. Mata-Calvo, J. Poliak, J. Surof, A. Reeves, M. Richerzhagen, H. F. Kelemu, R. Barrios, C. Carrizo, R. Wolf, F. Rein *et al.*, "Optical technologies for very high throughput satellite communications," in *Free-Space Laser Communications XXXI*, vol. 10910. SPIE, 2019.
- [7] P. Conroy, J. Surof, J. Poliak, and R. Mata-Calvo, "Demonstration of 40 gbaud intradyne transmission through worst-case atmospheric turbulence conditions for geostationary satellite uplink," *Appl. Opt.*, vol. 57, no. 18, pp. 5095–5101, 2018.
- [8] K. Saucke, C. Seiter, F. Heine, M. Gregory, D. Tröndle, E. Fischer, T. Berkefeld, M. Ferencik, M. Ferencik, I. Richter *et al.*, "The tesat transportable adaptive optical ground station," in *Int. Conf. on Space Optics (ICSO) 2016.*, vol. 9739. SPIE, 2016, p. 973906.
- [9] Y. Shoji, M. J. Fice, Y. Takayama, and A. J. Seeds, "A pilot-carrier coherent leo-to-ground downlink system using an optical injection phase lock loop (oipll) technique," *J. Lightw. Technol.*, vol. 30, no. 16, pp. 2696–2706, Aug 2012.
- [10] W. Rosenkranz and S. Schaefer, "Receiver design for optical inter-satellite links based on digital signal processing," in *18th IEEE Int. Conf. on Transparent Opt. Networks (ICTON)*, 2016, pp. 1–4.
- [11] T. Ando, E. Haraguchi, K. Tajima, Y. Hirano, T. Hanada, and S. Yamakawa, "Coherent homodyne receiver with a compensator of doppler shifts for inter orbit optical communication," in *Free-Space Laser Communication Technologies XXIII*, vol. 7923. SPIE, 2011, p. 79230J.
- [12] S. Schaefer, M. Gregory, and W. Rosenkranz, "Numerical investigation of a free-space optical coherent communication system based on optical phase-locked loop techniques for highspeed intersatellite data transmission," in *16th VDE-ITG Symp. on Photonic Networks*, 2015, pp. 69–74.
- [13] F. Roddier, *Adaptive optics in astronomy*. Cambridge Univ. Press, 1999.
- [14] E. A. Valencia, "Atmospheric compensation experiments on free-space optical coherent communication systems," Ph.D. dissertation, University of Barcelona, 2015.

- [15] U. Mengali and A. N. D'Andrea, *Synchronization techniques for digital receivers*. Kluwer Academic Publishers, 1997.
- [16] D. Divsalar, "Frequency correction," *Autonomous Software-Defined Radio Receivers for Deep Space Applications*, p. 63, 2006.
- [17] J. A. López-Salcedo, J. A. Del Peral-Rosado, and G. Seco-Granados, "Survey on robust carrier tracking techniques," *IEEE Commun. Surveys Tuts.*, vol. 16, no. 2, pp. 670–688, 2013.
- [18] L. Moller, "Novel aspects of spectral broadening due to fiber amplifier phase noise," *J. Quantum Electron.*, vol. 34, no. 9, pp. 1554–1558, 1998.
- [19] E. Rochat and R. Dandliker, "New investigations on the effect of fiber amplifier phase noise," *IEEE J. Sel. Topics Quantum Electron.*, vol. 7, no. 1, pp. 49–54, 2001.
- [20] I. Ricciardi, S. Mosca, P. Maddaloni, L. Santamaria, M. De Rosa, and P. De Natale, "Phase noise analysis of a 10 watt yb-doped fibre amplifier seeded by a 1-hz-linewidth laser," *Opt. Express*, vol. 21, no. 12, pp. 14 618–14 626, 2013.
- [21] G. C. Valley, "Isoplanatic degradation of tilt correction and short-term imaging systems," *Appl. Opt.*, vol. 19, no. 4, pp. 574–577, Feb 1980.
- [22] J. L. Bufton, "Comparison of vertical profile turbulence structure with stellar observations," *Appl. Opt.*, vol. 12, no. 8, pp. 1785–1793, 1973.
- [23] T. D. K. Kudielka, E. Fischer, "Numerical prediction and experimental validation of irradiance fluctuations in a pre-compensated optical feeder link," vol. 11180, 2019.
- [24] N. Védrenne, J.-M. Conan, M.-T. Velluet, M. Séchaud, M. Toyoshima, H. Takenaka, A. Guérin, and F. Lacoste, "Turbulence effects on bi-directional ground-to-satellite laser communication systems," in *IEEE Int. Conf. on Space Opt. Systems and Applications (ICSOS)*, 2012.
- [25] R. J. Noll, "Zernike polynomials and atmospheric turbulence\*," *J. Opt. Soc. Am.*, vol. 66, no. 3, pp. 207–211, Mar 1976.
- [26] N. A. Roddier, "Atmospheric wavefront simulation using zernike polynomials," *Opt. Eng.*, vol. 29, no. 10, pp. 1174–1181, 1990.
- [27] N. Védrenne, J.-M. Conan, C. Petit, and V. Michau, "Adaptive optics for high data rate satellite to ground laser link," vol. 9739, 2016.
- [28] M. Born and E. Wolf, *Principles of Optics, 6-th ed.* Pergamon, 1980.
- [29] S. Shaklan and F. Roddier, "Coupling starlight into single-mode fiber optics," *Appl. Opt.*, vol. 27, no. 11, pp. 2334–2338, 1988.
- [30] B. J. Klein and J. J. Degnan, "Optical antenna gain. 1: Transmitting antennas," *Appl. Opt.*, vol. 13, no. 9, pp. 2134–2141, 1974.
- [31] K. A. Winick, "Atmospheric turbulence-induced signal fades on optical heterodyne communication links," *Appl. Opt.*, vol. 25, no. 11, pp. 1817–1825, Jun 1986.
- [32] R. E. Wagner and W. J. Tomlinson, "Coupling efficiency of optics in single-mode fiber components," *Appl. Opt.*, vol. 21, no. 15, pp. 2671–2688, 1982.
- [33] C. Robert, J.-M. Conan, and P. Wolf, "Impact of turbulence on high-precision ground-satellite frequency transfer with two-way coherent optical links," *Phys. Rev. A*, vol. 93, p. 033860, Mar 2016.
- [34] S. Schaefer, M. Gregory, and W. Rosenkranz, "Coherent receiver design based on digital signal processing in optical high-speed intersatellite links with m-phase-shift keying," *Opt. Eng.*, vol. 55, no. 11, 2016.
- [35] K. Ho, *Phase modulated optical communication system*. Springer, 2005.
- [36] S. Saliba and R. Scholten, "Linewidths below 100 khz with external cavity diode lasers," *Appl. Opt.*, vol. 48, no. 36, pp. 6961–6966, 2009.
- [37] J. R. Barry and E. A. Lee, "Performance of coherent optical receivers," *Proc. IEEE*, vol. 78, no. 8, pp. 1369–1394, 1990.
- [38] J. Ohlson, "Exact dynamics of automatic gain control," *IEEE Trans. Commun.*, vol. 22, no. 1, pp. 72–75, January 1974.
- [39] M. Simon and J. Hamkins, "Carrier synchronization," *Autonomous Software-Defined Radio Receivers for Deep Space Applications*, 2006.
- [40] M. Simon, "On the optimality of the map estimation loop for carrier phase tracking bpsk and qpsk signals," *IEEE Trans. Commun.*, vol. 27, no. 1, pp. 158–165, January 1979.
- [41] F. M. Gardner, *Phaselock techniques*. John Wiley & Sons, 2005.
- [42] T. Hodgkinson, "Phase-locked-loop analysis for pilot carrier coherent optical receivers," *Elec. Lett.*, vol. 21, no. 25, pp. 1202–1203, 1985.
- [43] E. Agrell and M. Secondini, "Information-theoretic tools for optical communications engineers," in *IEEE Photonics Conf. (IPC)*, 2018.
- [44] V. Tikhonov, "The effect of noise on phase-lock oscillation operation," *Automatika i Telemekhanika*, vol. 20, no. 9, pp. 1188–1196, 1959.
- [45] T. Jesupret, M. Moeneclaey, and G. Ascheid, *Digital demodulator synchronization - Performance analysis*. Final report ESTEC contract nr. 8437/89/NL/RE, 1991.

**Laurie Paillier** received her M. Sc. in Optics Engineering at the Télécom Saint-Etienne Engineering School, Saint-Etienne, France, in 2017. She is currently pursuing her PhD in Optical Telecommunication at ONERA, the French Aerospace Lab, and the Institut Polytechnique de Paris, France, in collaboration with Télécom Paris, IMT-Atlantique and CNES. Her research focuses on space-to-ground optical coherent links using adaptive optics.

**Raphael Le Bidan (M'03)** received the Eng. Degree in Telecommunications and the M. Sc. Degree in Electrical Eng. from the Institut National des Sciences Appliquées (INSA), Rennes, France, in June 2000, and the Ph. D. degree in Electrical Eng. from the INSA, Rennes, in November 2003. Since December 2003, he has been working as an associate professor at IMT Atlantique (formerly ENST Bretagne), in the Signal & Communications dept. Current research interests focus on forward error correction and digital receiver design for coherent fiber and free-space optical transmission systems.

**Jean-Marc Conan** received the Ph.D. degree from Institut d'Optique Graduate School, France, in 1994. He has been working for more than 20 years in the High Angular Resolution unit of ONERA, the French Aerospace Lab, on modeling of turbulence optical effects, optimal control for adaptive optics, and wide field tomographic adaptive optics. Originally interested in astronomical imaging, he now explores other applications that benefit from this background: impact of turbulence on ground-space optical links for either high capacity telecommunications or high precision frequency transfer.

**Géraldine Artaud** has been working for CNES since 2006. She is working on space to earth high data rate communications in RF and optics. She is involved in the study of future systems using optical data transmissions for space. She is the responsible at CNES of the DOMINO demonstrator.

**Nicolas Védrenne** received the Ph.D degree from Nice-Sophia Antipolis University, France, in 2008. He is the manager of the High Angular Resolution unit of ONERA, the French Aerospace Lab. His research topics are optical wave propagation and adaptive optics. He was in charge of the development of TURANDOT, the wave optics code dedicated to the simulation of atmospheric turbulence on ground-satellite laser links. He is in charge of the FEDELIO project for ESA aiming at the experimental demonstration of the pre-compensation by adaptive optics for GEO feeder links.

**Yves Jauouën** received the Ph.D degree in Physics from Ecole Nationale Supérieure des Télécommunications (ENST), Paris, France in 1993. He joined the Communications and Electronic dept of Telecom Paris in 1982 where he is now a Professor. His present researches include high bit rate coherent optical communication systems, new characterization techniques for advanced photonic devices, high power fiber lasers, fiber optics and remote sensing. He is author or co-author of more 230 papers in journals and communications.